Determination of elastic moduli of rock samples using resonant ultrasound spectroscopy

TJ Ulrich and K. R. McCall
Department of Physics, University of Nevada, Reno, Nevada 89557

R. A. Guyer
Department of Physics, University of Massachusetts, Amherst, Massachusetts 01003

(Received 28 December 2000; revised 20 January 2002; accepted 28 January 2002)

Resonant ultrasound spectroscopy (RUS) is a method whereby the elastic tensor of a sample is extracted from a set of measured resonance frequencies. RUS has been used successfully to determine the elastic properties of single crystals and homogeneous samples. In this paper, we study the application of RUS to macroscopic samples of mesoscopically inhomogeneous materials, specifically rock. Particular attention is paid to five issues: the scale of mesoscopic inhomogeneity, imprecision in the figure of the sample, the effects of low Q, optimizing the data sets to extract the elastic tensor reliably, and sensitivity to anisotropy. Using modeling and empirical testing, we find that many of the difficulties associated with using RUS on mesoscopically inhomogeneous materials can be mitigated through the judicious choice of sample size and sample aspect ratio. © *2002 Acoustical Society of America.* [DOI: 10.1121/1.1463447]

PACS numbers: 43.35.Cg, 43.35.Yb, 43.20.Ks [SGK]

I. INTRODUCTION AND BACKGROUND

In this paper, we explore the application of resonant ultrasound spectroscopy (RUS) to macroscopic (e.g., $L_{\mathrm{macro}}=0.1$ cm–10 cm) samples of rock in order to learn the elastic tensor. Rocks are consolidated materials, typically assembled from aggregates of mesoscopic sized pieces (e.g., $L_{\mathrm{meso}}=10\ \mu$m–100 μm) of microscopically uniform material (length scale L_{μ}). They are mesoscopically inhomogeneous, that is, inhomogeneous on a scale small compared to the sample size but large compared to the microscopic length scale ($L_{\mathrm{macro}}\gg L_{\mathrm{meso}}\gg L_{\mu}$). Rocks are not easily machined to precise shapes. While the microscopic scale symmetry is homogenized by the process of their assembly, these samples may have macroscopic symmetry of great importance. For example, rock samples commonly have symmetry due to bedding planes or other features related to their construction. Our goal is to proscribe the conditions necessary for the successful use of RUS on rock and rocklike materials. These conditions include constraints on sample preparation and constraints on the set of reasonable questions that can be answered with RUS.

The success of RUS derives from the sensitivity of the normal mode frequencies of a sample to its elastic structure.[1] The elastic structure affecting resonance frequencies has three components: the figure of the sample; the homogeneity of the sample; and the elastic tensor of the sample, including symmetry and orientation. Given a perfectly homogeneous sample with a precise figure, the elastic tensor can be derived to a very high degree of accuracy.[2]

The definition of the elastic tensor C_{ijkl} comes from an expansion of the free energy of an elastic system to second order in the strain field,[3]

$$\mathcal{E}=\mathcal{E}_0+\tfrac{1}{2}C_{ijkl}\epsilon_{ij}\epsilon_{kl}, \tag{1}$$

where

$$\epsilon_{ij}=\frac{1}{2}\left(\frac{\partial u_i}{\partial x_j}+\frac{\partial u_j}{\partial x_i}\right) \tag{2}$$

is the $ij=ji$ component of the strain tensor, and u_i is the ith component of the displacement field. We use notation in which repeated indices are summed. The equation of motion for the displacement field is

$$\rho\frac{\partial^2 u_i}{\partial t^2}=\frac{\partial \sigma_{ij}}{\partial x_j}, \tag{3}$$

where

$$\sigma_{ij}=\frac{\partial \mathcal{E}}{\partial(\partial u_i/\partial x_j)} \tag{4}$$

is the stress field.

For a finite sample, the elastic equations of motion are complemented by the requirement that the normal components of internal stresses balance the external stresses at the surface of the sample. That is,

$$\sigma_{ik}(\mathbf{x})n_k(\mathbf{x})=P_i(\mathbf{x}), \tag{5}$$

where $\mathbf{n}$ is the normal to the surface at $\mathbf{x}$, and P_i is the normal component of the external stress applied to the sample at $\mathbf{x}$.

For linear systems, the elastic tensor C_{ijkl} relates the stress field to the strain field, $\sigma_{ij}=C_{ijkl}\epsilon_{kl}$. Because both stress and strain are symmetric, $\sigma_{ij}=\sigma_{ji}$ and $\epsilon_{ij}=\epsilon_{ji}$, the notation is commonly contracted such that stress and strain are six-component rank-one tensors, and the elastic tensor is a 6×6 rank-two tensor.[4] In the contracted notation,

$$\sigma_{\alpha}=c_{\alpha\beta}\epsilon_{\beta}, \tag{6}$$

where $x=1$, $y=2$, $z=3$, $\epsilon_{11}=\epsilon_1$, $\epsilon_{22}=\epsilon_2$, $\epsilon_{33}=\epsilon_3$, $\epsilon_{23}=\epsilon_4$, $\epsilon_{31}=\epsilon_5$, $\epsilon_{12}=\epsilon_6$, and similarly for the stresses. For an isotropic sample, the symmetry of the system allows further

reductions of the elastic tensor until only two elements are independent,

$$c_{\alpha\beta}=\begin{pmatrix} \lambda+2\mu & \lambda & \lambda & 0 & 0 & 0 \\ \lambda & \lambda+2\mu & \lambda & 0 & 0 & 0 \\ \lambda & \lambda & \lambda+2\mu & 0 & 0 & 0 \\ 0 & 0 & 0 & \mu & 0 & 0 \\ 0 & 0 & 0 & 0 & \mu & 0 \\ 0 & 0 & 0 & 0 & 0 & \mu \end{pmatrix}, \quad (7)$$

or $c_{11}=\lambda+2\mu$, $c_{12}=\lambda$, and $c_{44}=\mu=(c_{11}-c_{12})/2$. The constants λ and μ are called the Lamé coefficients; c_{11} is the compressional modulus, and c_{44} is the shear modulus (μ). Other sets of two independent coefficients are also common, such as the bulk modulus and shear modulus ($K=\lambda+2\mu/3, G=\mu$), or Young's modulus and Poisson's ratio [$E=\mu(3\lambda+2\mu)/(\lambda+\mu), \nu=\lambda/2(\lambda+\mu)$].

In terms of the Lamé coefficients, the equation of motion, Eq. (3), for an isotropic sample is

$$\rho\ddot{u}_i=(\lambda+\mu)\frac{\partial}{\partial x_i}\nabla\cdot\mathbf{u}+\mu\nabla^2 u_i, \quad (8)$$

and the boundary condition on the surface of the sample is

$$\lambda\nabla\cdot\mathbf{u}n_i+2\mu\frac{\partial u_i}{\partial x_k}n_k=P_i; \quad (9)$$

$P_i=0$ for a free standing sample.

Historically, the elements of the elastic tensor of macroscopic inhomogeneous materials have been found using mechanical testing[5] or ultrasonic time-of-flight measurements.[6] In mechanical testing the strain in response to stress, the inverse of Eq. (6), is measured between ambient conditions and failure in order to determine material strength and toughness. Components of the elastic tensor are found from mechanical testing data as the slope of stress versus strain extrapolated to low strain. For example, $c_{11}=\sigma_1/\epsilon_1$, for low strain. A mechanical test is typically quasistatic, i.e., the stress is varied slowly (e.g., 0 MPa to 10 MPa in 1000 s). Mechanical tests are inherently high amplitude tests. The great disadvantage to using such tests to determine the low strain elastic tensor is that the sample is often altered or destroyed as a result of the test. Thus results cannot be confirmed for a given sample and only part of the elastic tensor can be determined for each run. In addition, mechanical testing often probes the sample at strains that activate its hysteretic elastic response. Thus extrapolation of such data to low strain is not reliable.[7] Our primary interest is in the elastic tensor for low amplitude disturbances that is related to the propagation of acoustic waves. Generally, elements of the elastic tensor found from mechanical testing have lower value than elements of the elastic tensor inferred from time-of-flight measurements. In other words, the quasistatic modulus is less than the dynamic modulus.

Time-of-flight determinations of the elements of the elastic tensor are measurements of the velocity of an acoustic pulse propagating in the sample. The displacement caused by the acoustic pulse obeys Eq. (8), but the constraints set by Eq. (9) at the sample surface are not met, as transducers must be bonded to the surfaces of the sample. The boundary condition can be ignored if the pulse width is small compared to the sample width. The transmission time t of an ultrasonic pulse across the sample is measured. Given the distance from source to receiver L, and density of the sample ρ, the wave velocities and elastic tensor can be determined. From $v=L/t$, $c_{11}=\lambda+2\mu=\rho v_c^2$, and $c_{44}=\mu=\rho v_s^2$, where v_c and v_s are the compressional wave velocity (wave vector parallel to displacement) and shear wave velocity (wave vector perpendicular to displacement) respectively. To determine both compressional and shear velocities, transducers that produce compressional and shear waves are bonded to the sample in a variety of orientations.

Resonant ultrasound spectroscopy is an alternative technique for determining the elements of the elastic tensor of a sample. In RUS the frequencies of N low-lying modes of a free standing sample are measured. These measured frequencies are compared to N frequencies found by solving Eq. (8), while satisfying the free boundary condition set by Eq. (9) with $P_i=0$. The modes of the sample are not simply compressional or shear waves, as is the case for pulse propagation, but are complicated entities having both compressional and shear character. Thus in RUS the problem of solving Eqs. (8) and (9) for the nth model resonance frequency f_n^M, has equal prominence with the problem of measuring the nth experimental resonance frequency f_n^X. The elements of the elastic tensor are found by minimizing

$$df^2=\sum_{n=1}^{N}(f_n^X-f_n^M(c_{\alpha\beta}))^2 \quad (10)$$

with respect to $c_{\alpha\beta}$.

In Sec. II, several issues pertaining to using RUS on inhomogeneous samples are discussed. In most cases, numerical modeling was used to explore ways to optimize experimental chances for success. In Sec. III, the results of RUS experiments on a variety of samples are displayed and discussed as well as a summary of our findings, describing the bounds on RUS applicability to inhomogeneous materials found empirically and through modeling.

II. MODELING AND EXPERIMENTAL DEVELOPMENT

In this section we will apply the methods described in Visscher *et al.*[8] to model and analyze experiments performed on macroscopic samples of rock. The assumptions inherent in the analysis will be discussed, as well as ways in which to maximize the success of RUS on samples whose properties do not superficially satisfy these assumptions. Since rocks are not single crystals, or even polycrystals, but are usually aggregates of multiple materials with different symmetry properties, we do not expect to be able to study detailed properties of specific modes of the sample, or to probe the sophisticated symmetries that may be present in the constituents of the samples. Our goal is to characterize the aggregate material. To this end, we will focus our attention on average frequency changes over multiple modes, i.e., we begin by answering the broadest questions, such as whether there is a good isotropic approximation to the elastic tensor of the rock. If we have a satisfactory answer to this question, we

may ask whether there is a possible transverse isotropic approximation to the elastic tensor. In this work, we do not attempt to answer refined questions that focus on the behavior of particular modes of a particular symmetry.

The experiment, measurement of resonance frequencies, and numerical inversion is performed using hardware and software developed by Dynamic Resonance Systems (DRS), a commercial provider of RUS measurement systems. Numerical inversion, i.e., determination of $c_{\alpha\beta}$ from Eq. (10), is based on the Visscher *et al.*[8] variational technique. The analysis software finds model resonance frequencies using a model of the elastic system in which it is (A) free standing, (B) spatially homogeneous, and (C) a rectangular parallelepiped. Departure of the experimental system or sample from these three conditions can introduce shifts in the experimentally measured frequencies that will introduce errors in the derived elastic tensor. How well our system and samples conform to (A), (B), and (C), and estimates of the error induced by nonconformity are discussed below.

Rock and similar type samples, e.g., concrete, have relatively high acoustic attenuation, or low Q. Thus several very practical issues arise. (D) What can we do to make the resonance peaks distinct from one another and therefore well defined? (E) How do we acquire the most information out of the low-lying resonance peaks, the ones we can see clearly? That is, how do we maximize the dependence of the low-lying resonances on the full elastic tensor? Finally, (F) how sensitive are we to anisotropy in the sample? We will show here, that by altering the sample geometry, while maintaining a rectangular parallelepiped shape, these practical issues can be addressed.

A. Free boundaries

The variational technique used to find model frequencies, f_n^M, is based on recognizing that the displacement field satisfying the elastic wave equation with free boundaries on the sample surface, Eq. (8) and Eq. (9) with $P_i=0$, also makes the elastic Lagrangian of the sample stationary.[8] To approximate free boundaries in the experiment, the source and detector are most often placed at vertices of the parallelpiped, delicately supporting the sample. The sample is nearly free standing. Holding the sample at vertices has the further advantage of keeping the transducers away from the expected node lines of the resonant modes. When the full resonance spectrum is complicated, transducers may be placed purposely at expected nodes, such as the center of a face, to temporarily simplify the spectrum. Using transducers for support limits the sample size. Our transducers are PZT-5 piezoelectric pinducers. We have limited our samples to less than 100 cm^3, and 250 g.

B. Homogeneity

The elastic behavior of a consolidated material is primarily determined by a macroscopic average over the bonds between constituents (grains in a rock), rather than by the elastic properties of the constituents themselves. For example, the elastic behavior of sandstone, a quartz conglomerate, is more a function of grain-to-grain bond properties than of SiO_2 properties. We are interested in the elastic properties of consolidated materials, i.e., materials that are mesoscopically inhomogeneous. We want to be able to regard these materials as homogeneous. We adopt the rule of thumb that an inhomogeneous material looks homogeneous to a propagating wave when the wavelength of the wave is much greater than the length scale of the inhomogeneity.

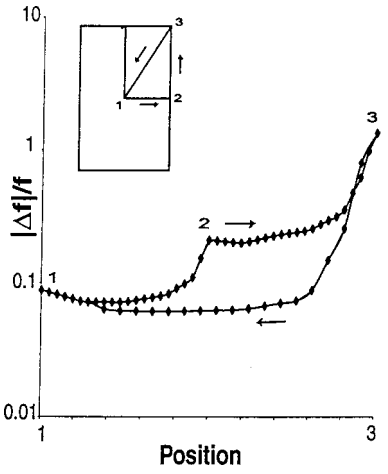

FIG. 1. Percentage frequency shift as a function of mass perturbation placement. The perturbation is moved through a two-dimensional rectangle as shown in the inset.

A simple calculation for a one-dimensional system with free boundaries results in resonance wavelengths $\lambda=2l/n$, where l is the length of the sample and n is an integer number of nodes. Assuming that we need the first ten resonance frequencies to accurately determine two elastic constants with RUS,[1] we want the maximum size of an inhomogeneity $\xi \ll l_{\min}/5$, where $l_{\min}$ is the length of the smallest side of the sample. This estimate is very conservative, since it is highly unlikely that all of the first ten resonant modes in a three-dimensional sample will have nodes along a single direction. We use the ratio $\xi/l_{\min}$ to characterize the inhomogeneity of our samples, where ξ is crudely determined by measuring the diameter of the largest area of color variation on the surface of a sample, e.g., the diameter of the largest black spot on a sample of Sierra white granite.

C. Sample geometry, the figure of the sample

Samples of consolidated materials are difficult to machine without chipping, and often do not have perfectly parallel sides. How ideal must the figure of a sample be? This question can be examined using the perturbation treatment of the elasticity problem sketched in the Appendix. To simulate the effect of an error in the figure of a sample, a localized mass is carried around a two-dimensional rectangular membrane, and the frequency shift caused by this mass is calculated. The frequency shift for mode n is given by

$$\frac{\omega_n^2-\omega_{n0}^2}{\omega_{n0}^2}\approx 2\,\frac{\delta f_n}{f_n}=\langle u_n|\frac{\delta\rho}{\rho_0}|u_n\rangle, \tag{11}$$

where u_n and ω_{n0} are the nth eigenmode and eigenfrequency of a perfectly shaped sample and $\delta\rho$ is the localized mass perturbation being carried around the sample (see the Appendix). In Fig. 1, the average frequency shift of the lowest 20

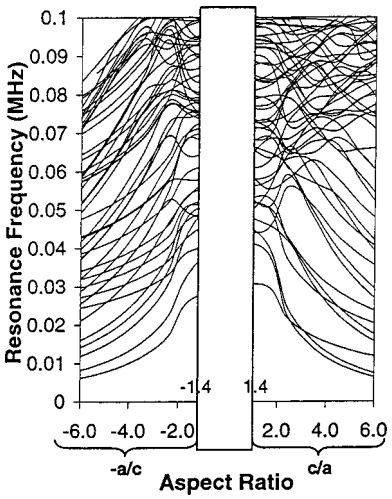

FIG. 2. Calculated resonance frequencies as a function of aspect ratio. The sample is at a constant volume of 4.8 cm^3; $b=1.1a$, and the aspect ratio is c/a on the right side, $-a/c$ on the left side. The elastic constants are $c_{11}=86.6$ GPa and $c_{44}=31.9$ GPa.

resonances of the membrane,

$$\delta F=\frac{1}{20}\sqrt{\sum_{n=1}^{20}\left(\frac{\delta f_n}{f_n}\right)^2}, \tag{12}$$

is shown as a function of the perturbation placement. The perturbation is carried along the sample edge and into the sample interior as shown in the inset in the figure. When the perturbation is at an interior point it is essentially a 1% mass distortion, when it is along the perimeter it is a 1% distortion of the figure. Distortions in the figure of the sample are much more important than equivalent mass distortions in the sample interior. A 1% chip out of the corner of a sample can produce a 1% change in the frequency. A 1% mass distortion at the sample center produces less than 0.2% change in frequency.

The test calculation was performed on a two-dimensional membrane. In three dimensions we expect small mass distortions to cause smaller frequency shifts than in two dimensions. Given the number of other contributors to error in RUS measurements on consolidated materials, the contribution due to a mass or figure distortion is rather small. This conclusion was confirmed empirically by making RUS measurements on samples before and after chipping, and on various samples of the same size.

D. Distinct resonance peaks

Consolidated materials are often found to have a low quality factor Q, i.e., a high attenuation. At fixed amplitude, low Q materials have fewer observable resonance frequencies than high Q materials. Additionally the broader resonance peaks of low Q materials overlap nearby peaks and complicate peak picking. However, the geometry of a sample sets the frequency difference between peaks. For example, a sample that is a cube of an isotropic material has a three-fold degeneracy in all of its resonance frequencies. Thus we can use geometry to minimize peak overlap due to a low Q.

In Fig. 2, calculated resonance frequencies are plotted for a parallelepiped sample as a function of the aspect ratio, c/a. The volume of the sample is fixed, $a\times b\times c=4.8$ cm^3, and $b=1.1a$. Aspect ratios greater than one correspond to rodlike samples and are characterized by the number c/a in Fig. 2. Aspect ratios less than one correspond to platelike samples and are characterized by the number $-a/c$ in Fig. 2. A homogeneous, isotropic sample with elastic constants appropriate to basalt was assumed. As the aspect ratio is increased, the low-lying modes separate. For example, at $b=1.1a$, $c/a=4$, we expect to be able to pick out 14 distinct resonances before mode overlap becomes a serious problem for a RUS experiment.

Increasing the aspect ratio further might allow us to pick out even more distinct peaks. However, the RUS inversion code uses a fixed order polynomial to variationally fit modes.[8] As one side of a sample becomes disproportionately large, a disproportionate number of nodes in the normal modes will be in that direction, and the inversion code will lose fitting accuracy in that direction. We have chosen to keep samples at $1/4\leqslant c/a\leqslant 4$ (-4 to 4 in Fig. 2).

E. c_{11} dependence

A rule of thumb[1] is that five resonance frequencies are needed to accurately determine each independent component of the elastic tensor. Thus for an isotropic material described by two independent components, c_{11} and c_{44}, we need to experimentally determine at least ten resonance frequencies. Certainly the confidence with which the two independent components of the elastic tensor can be determined is influenced by the involvement of each component in the first ten modes of the sample.

The dependence of mode n on c_{11} or c_{44} is given by the derivative of the nth model frequency with respect to the modulus,

$$D_{in}=\frac{2c_{ii}}{f_n^M}\frac{\partial f_n^M}{\partial c_{ii}}, \tag{13}$$

where $i=1$, or 4. The derivatives are normed such that $D_{1n}+D_{4n}=1$. Since $c_{44}\approx c_{11}/2$, i.e., $v_s<v_c$, we expect low frequency modes to be more highly dependent on c_{44} than on c_{11} (in analogy to the frequencies of the modes of a soft spring versus a stiff spring network). Indeed, for a cube of basalt, the first eight modes have an average dependence on c_{11} of less than 15%. That is, most low-lying modes are shear modes, involving very little compression. However, the geometry of the sample influences the dependence of a mode on c_{11}. Platelike and rodlike samples will have low-lying bending or flexural modes that are compressional in nature.

In Fig. 3, the mode dependence on c_{11}, D_{1n}, is shown as a function of the ratio of the longest side to the shortest side of the sample, c/a, for the first ten modes of a parallelepiped. The third side of the sample is held fixed with respect to the shortest side, $b=1.1a$. Positive aspect ratios denote rodlike samples (the aspect ratio c/a on the right side); negative aspect ratios denote platelike samples (the aspect ratio $-a/c$ on the left side). A homogeneous, isotropic sample with elastic tensor appropriate to basalt was used. As the aspect ratio is increased, sensitivity to c_{11} increases. For ex-

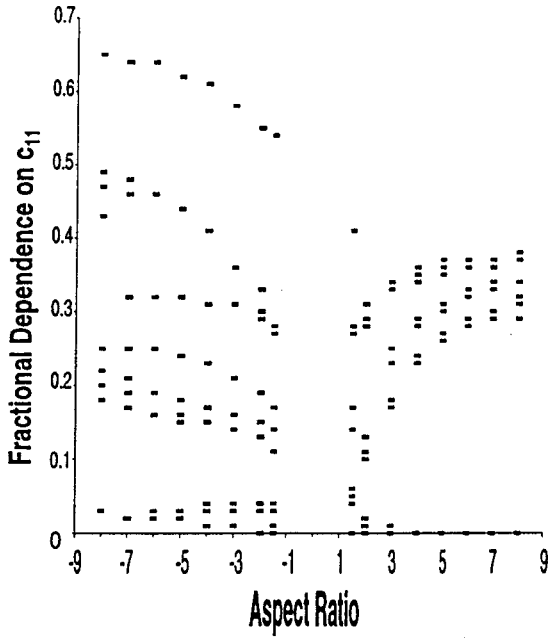

FIG. 3. c_{11} dependence as a function of aspect ratio. The sample is at a constant volume of 4.8 cm^3; $b=1.1a$, and the aspect ratio is c/a on the right side, $-a/c$ on the left side. The elastic constants are $c_{11}=86.6$ GPa and $c_{44}=31.9$ GPa.

ample, for a sample with $c/a=4$, seven of the first ten modes have a c_{11} dependence over 20%, as opposed to only two modes for $c/a=1$.

F. Anisotropy

If isotropic symmetry is broken in a single direction, the sample has hexagonal symmetry and is called transversely isotropic. Many consolidated materials, such as sedimentary rock and laminar systems, are transversely isotropic. The elastic tensor of a system with hexagonal symmetry has five independent elements: c_{11}, c_{33}, c_{13}, c_{44}, and c_{66}. Thus in order to determine the elastic tensor for a system with hexagonal symmetry, we might expect to need 25 resonance frequencies. This is a prohibitively large number for low Q samples. Can we detect anisotropy with the lowest 10 modes? The following is a test of the sensitivity of RUS to anisotropy.

Consider a hexagonal elastic tensor

$$M=\begin{pmatrix} c_{11} & c_{12} & c_{13} & 0 & 0 & 0 \\ c_{12} & c_{11} & c_{13} & 0 & 0 & 0 \\ c_{13} & c_{13} & c_{33} & 0 & 0 & 0 \\ 0 & 0 & 0 & c_{44} & 0 & 0 \\ 0 & 0 & 0 & 0 & c_{44} & 0 \\ 0 & 0 & 0 & 0 & 0 & c_{66} \end{pmatrix}, \tag{14}$$

where

$$c_{11}=(1+\epsilon)C_0, \tag{15}$$

$$c_{12}=0.4(1-2\epsilon)C_0, \tag{16}$$

$$c_{13}=0.4(1+\epsilon)C_0, \tag{17}$$

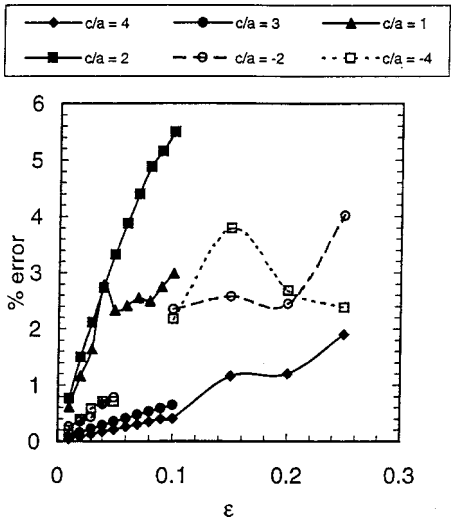

FIG. 4. Root-mean-square error for an isotropic fit to anisotropic sample resonances. Anisotropy is characterized by the parameter ϵ. RUS fits are performed for $c/a=-4,-2,1,2,3,4$.

$$c_{33}=(1-2\epsilon)C_0, \tag{18}$$

$$c_{44}=0.3(1-1.5\epsilon)C_0, \tag{19}$$

$$c_{66}=0.3(1+3\epsilon)C_0. \tag{20}$$

As ϵ varies from 0 to 0.25, the elastic tensor varies from isotropic to hexagonal. Independent of ϵ, $c_{11}+c_{22}+c_{33}=3C_0$; $c_{12}+c_{13}+c_{23}=1.2C_0$; and $c_{44}+c_{55}+c_{66}=0.9C_0$. For $\epsilon=0.25$ the elements of the elastic tensor have relative values approximately that of zinc.[9]

Sensitivity to anisotropy is calculated as follows: (1) Choose values of c/a, and ϵ. (2) Calculate the lowest 10 resonance frequencies of the hexagonal system, using the elastic tensor in Eqs. (14)–(20), and call these frequencies the experimentally measured frequencies f_n^X. (3) Fit these frequencies f_n^X with an isotropic model, i.e., minimize Eq. (10) assuming that the f_n^M depend only on c_{11} and c_{44}.

In Fig. 4 the rms frequency error,

$$\text{rms error}=\sqrt{\frac{1}{10}\sum_{n=1}^{10}\left(\frac{f_n^X-f_n^M}{f_n^X}\right)^2}, \tag{21}$$

is shown as a function of ϵ, for various aspect ratios c/a, and $b/a=1.1$. In the figure, aspect ratios less than one are represented as negative reciprocals, e.g., $c/a=1/4$ is represented as $c/a=-4$. For $c/a=4$, the rms error is less than 1% for $\epsilon<0.22$. If we choose 1% error as the threshold between a good fit and a bad fit, we do not have enough information about the elastic properties of the system to recognize that it is anisotropic if we are given only the first ten modes. For $c/a=2$, the rms error rises fastest as the degree of anisotropy increases. This implies that the $c/a=2$ aspect ratio provides the best detection of anisotropy. However, the ability to accurately determine the elastic tensor for an anisotropic sample will still depend on having a data set with 20 or more resonance frequencies.

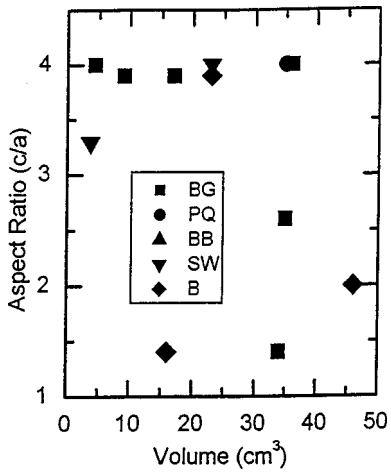

FIG. 5. Aspect ratio as a function of volume for the 13 samples studied. Samples are black gabbro (BG), pink quartzite (PQ), Berkeley blue granite (BB), Sierra white granite (SW), and basalt (B).

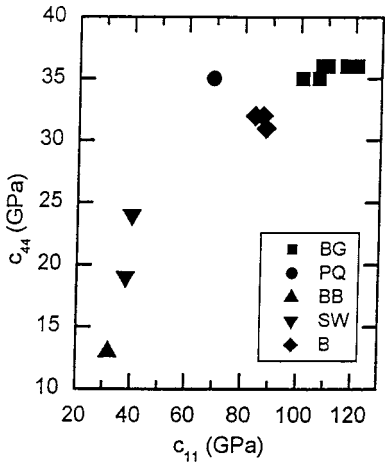

FIG. 6. c_{11} versus c_{44} for the 13 samples studied. Samples are black gabbro (BG), pink quartzite (PQ), Berkeley blue granite (BB), Sierra white granite (SW), and basalt (B).

III. RESULTS AND CONCLUSIONS

The previous section has provided a foundation for the investigation of real samples. RUS experiments and analysis were performed on five rock types. The sample set consists of 13 parallelepipeds: 6 of Berkeley blue granite, 1 of pink quartzite, 1 black gabbro, 2 of Sierra white granite, and 3 of basalt. Multiple samples of the same rock type were cut from a single large specimen. Figure 5 shows the aspect ratios and volumes spanned by the sample set.

For each sample, an estimate of the expected isotropic elastic tensor was used to calculate the expected (model) resonance frequencies for the sample. These model frequencies were used to guide the experimental search for resonances. RUS scans were performed for each sample to find the first ten experimental resonance frequencies. The first ten visible experimental resonant modes are not always the first ten modes as predicted by the model, i.e., some modes are missing in the experiment. Thus while the data analysis was always performed with ten experimentally measured resonance frequencies, the mode identities are not necessarily the same from sample to sample.

Table I contains the RUS derived elements of the isotropic elastic tensors of the 13 samples. The reported value of Q is the average quality factor for the lowest ten measured resonance frequencies,

$$Q=\frac{1}{10}\sum_{n=1}^{10}\frac{f_n^X}{\Delta f_n^X}, \tag{22}$$

where Δf_n^X is the full-width at half-maximum of the resonance intensity centered at f_n^X. The error in the right-most column is given by Eq. (21). The isotropic moduli derived for each sample, c_{11} and c_{44} are also shown in Fig. 6.

Notice that for all black gabbro samples, the shear modulus (c_{44}) is consistently 35–36 GPa, while the compressional modulus (c_{11}) varies by 20%. As indicated in the percent c_{11} column of the table, the compressional modulus varies because it is not heavily involved in the resonant modes used for the fits (Sec. II E). The smallest aspect ratio black gabbro sample has the largest rms frequency error, as expected. However, there is no direct correlation between rms frequency error and aspect ratio. Too many other factors play a role, such as volume and the presence of inhomoge-

TABLE I. Sample set 1. Samples are black gabbro (BG), pink quartzite (PQ), Berkeley blue granite (BB), Sierra white granite (SW), and basalt (B). The samples are characterized by smallest side a, aspect ratio c/a, volume V, relative size of inhomogeneity ξ/a, quality factor Q, compressional modulus c_{11}, percentage of compressional modulus involvement in the ten modes used for the fit, shear modulus c_{44}, and rms error in the RUS fit to resonance frequencies.

Sample	a (cm)	c/a	V (cm^3)	ξ/a	Q	c_{11} (GPa)	$\%c_{11}$	c_{44} (GPa)	% error
BG-1	2.8	1.4	34	0.23	350	101	14	35	1.23
BG-2	2.3	2.6	35	0.28	350	108	12	36	0.27
BG-3	1.0	4.0	4.4	0.32	350	121	14	36	0.48
BG-4	1.3	3.9	9.1	0.24	350	107	16	35	0.39
BG-5	1.6	3.9	17	0.31	350	117	10	36	0.71
BG-6	2.0	4.0	36	0.21	350	110	16	36	0.31
PQ	2.0	4.0	35	1.7	250	69	42	35	1.4
BB	2.0	4.0	35	0.20	230	32	26	13	13
SW-1	0.96	3.3	3.7	0.46	150	40	51	24	15
SW-2	1.7	4.0	23	0.17	140	38	54	19	0.61
B-1	2.1	1.4	16	0.29	275	88	13	31	0.69
B-2	2.8	2.0	46	0.04	255	84	14	32	0.47
B-3	1.7	3.9	23	0.06	335	87	20	32	0.31

neity. An important factor in RUS experiments, that cannot be easily quantified, is user confidence. While the results of a RUS fit may not provide direct evidence that a high aspect ratio sample gives better results than a low aspect ratio sample, the picking of the resonance peaks (accomplished primarily by hand and eye) is easier for high aspect ratios, since the peaks are more spread out (Fig. 2).

If we require that the rms frequency error in the RUS fits be less than 1%, the results from BG-1, BB, and SW-1 would be considered invalid. Notice that the elastic tensors derived for the two Sierra white granite samples are within 20% of each other, even though the rms frequency errors are wildly different. Again, the rms frequency error is not a reliable test of the validity of results. Indeed, the commonly accepted values of the moduli of Berkeley blue granite are $c_{11}=30$ GPa and $c_{44}=13$ GPa. Given inherent variability in samples, and the low dependence of the measured resonant modes on c_{11}, the results for Berkeley blue granite are remarkably good. The rms frequency error is not directly correlated with any of the variables we studied, i.e., aspect ratio, volume, Q, or relative inhomogeneity. However, it is still a measure of how well our experimental RUS results can be modeled.

The modeling in Sec. II and the results shown in Table I indicate that RUS is a viable technique for characterizing the average elastic behavior of inhomogeneous materials. Although larger rms errors can be expected for inhomogeneous materials than those acceptable for homogeneous samples (less than 0.5%[1]), our results are generally close for different samples of the same material, and consistent with accepted values.[10] We have found that high aspect ratio samples are easier to work with than low aspect ratio samples, although our results indicate that this is primarily a user preference issue, rather than an accuracy issue. A hypothesis that remains untested is whether anisotropy is more likely to be detected with low aspect ratio samples than with high aspect ratio samples.

The future of RUS as a characterization tool for inhomogeneous materials may be more connected to the sensitivity of resonant modes to changes in the elastic state of a system, than to the ability of the RUS inversion technique to accurately predict the elastic tensor. Preliminary measurements of resonances of Berea sandstone as a function of temperature, show that the elastic behavior of Berea sandstone at low temperature (less than 200 K) is repeatably hysteretic.[11,12] These measurements also indicate that the elastic tensor is softening, rather than hardening, as the temperature is lowered. RUS may prove to be a useful technique for probing changes in elastic state under extreme conditions.

ACKNOWLEDGMENTS

The authors acknowledge useful discussions with T. W. Darling, A. Migliori, and P. A. Johnson. This work was sponsored by the Department of the Navy, Office of Naval Research, and the Institute for Geophysics and Planetary Physics, Los Alamos National Laboratory.

APPENDIX: PERTURBATION THEORY FOR NONIDEAL SAMPLE GEOMETRY

The elastic energy of a solid body, in steady state at frequency ω, is described by the Lagrangian

$$L=\int d\mathbf{x}\phi(\mathbf{x})\left(\frac{\omega^2}{2}\rho(\mathbf{x})u_i^2-\frac{1}{2}c_{ijkl}(\mathbf{x})\frac{\partial u_i}{\partial x_j}\frac{\partial u_k}{\partial x_l}\right), \quad \text{(A1)}$$

where $\mathbf{u}$ is the displacement vector at position $\mathbf{x}$, c_{ijkl} is the elastic tensor, ρ the mass density, repeated indices are summed over the Cartesian coordinates, and ϕ describes the extent or figure of the sample,

$$\phi(\mathbf{x})=\begin{cases}1, & \mathbf{x} \text{ inside the sample}\\ 0, & \mathbf{x} \text{ outside the sample.}\end{cases} \quad \text{(A2)}$$

Equation (A1) is quite general, allowing for: (1) an arbitrary sample figure $\phi(\mathbf{x})$; (2) a nonuniform density $\rho(\mathbf{x})$; and (3) a nonuniform elastic tensor $c_{ijkl}(\mathbf{x})$.

The equation of motion for the normal modes is found by varying L with respect to u_i. If the traction on the surfaces defined by $\phi(\mathbf{x})$ vanishes, u_i satisfies a wave equation in the form

$$\rho(\mathbf{x})\omega^2u_i+\frac{\partial}{\partial x_j}\left(c_{ijkl}(\mathbf{x})\frac{\partial u_k}{\partial x_l}\right)=0 \quad \text{(A3)}$$

for $\mathbf{x}$ inside the sample. The condition that the traction on the surfaces vanish is enforced by holding the sample so that it is effectively free standing.

The equation of motion for u_i, Eq. (A3), can be cast in the form of a variational problem.[11] That is, the quantity $\omega^2[u_i]$, where

$$\omega^2[u_i]=\frac{\int d\mathbf{x}\phi(\mathbf{x})c_{ijkl}(\mathbf{x})\partial u_i/\partial x_j\,\partial u_k/\partial x_l}{\int d\mathbf{x}\phi(\mathbf{x})\rho(\mathbf{x})u_i^2}, \quad \text{(A4)}$$

must be stationary subject to arbitrary variations of u_i consistent with traction free boundaries. Using this form for the normal mode frequencies it is possible to make a systematic study of the consequences of change in $\phi(\mathbf{x})$, $\rho(\mathbf{x})$, and $c_{ijkl}(\mathbf{x})$. Assume the ideal sample is a rectangular parallelepiped specified by ϕ_0, has uniform density ρ_0, and has uniform elastic constants c^0_{ijkl}. Then variations in these quantities are given by $\delta\phi(\mathbf{x})=\phi(\mathbf{x})-\phi_0$, $\delta\rho(\mathbf{x})=\rho(\mathbf{x})-\rho_0$, and $\delta c_{ijkl}(\mathbf{x})=c_{ijkl}(\mathbf{x})-c^0_{ijkl}$. To first order in $\delta\phi$, $\delta\rho$, and δc we have

$$\omega^2=\frac{N_0}{D_0}\left[1+\frac{\delta N_c}{N_0}+\frac{\delta N_\phi}{N_0}-\frac{\delta D_\rho}{D_0}-\frac{\delta D_\phi}{D_0}\right], \quad \text{(A5)}$$

where

$$N_0=c^0_{ijkl}\int d\mathbf{x}\phi_0\frac{\partial u_i}{\partial x_j}\frac{\partial u_k}{\partial x_l}. \quad \text{(A6)}$$

$$D_0=\rho_0\int d\mathbf{x}\phi_0u_i^2, \quad \text{(A7)}$$

$$\delta N_c=\int d\mathbf{x}\phi_0\delta c_{ijkl}(\mathbf{x})\frac{\partial u_i}{\partial x_j}\frac{\partial u_k}{\partial x_l}, \quad \text{(A8)}$$

$$\delta N_\phi=c^0_{ijkl}\int d\mathbf{x}\delta\phi(\mathbf{x})\frac{\partial u_i}{\partial x_j}\frac{\partial u_k}{\partial x_l}, \quad \text{(A9)}$$

$$\delta D_p = \int d\mathbf{x}\phi_0 \delta\rho(\mathbf{x}) u_i^2, \tag{A10}$$

$$\delta D_\phi = \rho_0 \int d\mathbf{x}\delta\phi(\mathbf{x}) u_i^2. \tag{A11}$$

Using the variational technique of Visscher *et al.*, we can find the eigenvalues $\omega_{\nu,0}^2 = N_0/D_0$ and eigenfunctions $u_{i,\nu}^0 = \psi_\nu(\mathbf{x})$ associated with the ideal sample. Thus the lowest order contribution to the frequency shift due to a perturbation is

$$\frac{\omega_\nu^2 - \omega_{\nu,0}^2}{\omega_{\nu,0}^2} = \frac{\delta N_c}{N_0} + \frac{\delta N_\phi}{N_0} - \frac{\delta D_\rho}{D_0} - \frac{\delta D_\phi}{N_0}, \tag{A12}$$

where $u_i = \psi_\nu(\mathbf{x})$. For the example of an inhomogeneous mass density, we would have

$$\frac{\omega_\nu^2 - \omega_{\nu,0}^2}{\omega_{\nu,0}^2} = -\frac{\int d\mathbf{x}\phi_0 \delta\rho(\mathbf{x}) |\psi_\nu|^2}{\rho_0 \int d\mathbf{x}\phi_0 |\psi_\nu|^2}, \tag{A13}$$

where

$$\omega_{\nu,0}^2 = \frac{c_{ijkl}^0 \int d\mathbf{x}\phi_0 \partial\psi_\nu/\partial x_j \, \partial\psi_\nu/\partial x_l}{\rho_0 \int d\mathbf{x}\phi_0 |\psi_\nu|^2}. \tag{A14}$$

Equation (A13) is used in Sec. II C for the case of a mass defect to illustrate the consequences of a mass inhomogeneity on resonant mode frequencies of a two-dimensional membrane.

[1] A. Migliori and J. L. Sarrao, *Resonant Ultrasound Spectroscopy* (Wiley, New York, 1997).

[2] J. L. Sarrao, D. Mandrus, A. Migliori, Z. Fisk, I. Tanaka, H. Kojima, P. C. Canfield, and P. D. Kodali, "Complete elastic moduli of $La_{2-x}Sr_xCuO_4$ ($x = 0.00$ and 0.14) near the tetragonal-orthorhombic structural phase transition," Phys. Rev. B **50**, 13125–13131 (1994).

[3] L. D. Landau and E. M. Lifshitz, *Theory of Elasticity*, 3rd ed. (Pergamon, Oxford, 1986), pp. 9–11.

[4] R. E. Green, Jr., *Treatise on Materials Science and Technology, Vol. 3, Ultrasonic Investigation of Mechanical Properties* (Academic, New York, 1973), pp. 76–78.

[5] F. Birch, "Compressibility; Elastic Constants," in *Handbook of Physical Constants*, edited by S. P. Clark (Geological Society of America, New York, 1966), Vol. 97, pp. 97–106.

[6] T. Bourbie, O. Coussy, and B. Zinszner, *Acoustics of Porous Media* (Gulf Publishing, Houston, 1987), pp. 145–169.

[7] R. A. Guyer, K. R. McCall, G. N. Boitnott, L. B. Hilbert, Jr., and T. J. Plona, "Quantitative implementation of Preisach–Mayergoyz space to find static and dynamic elastic moduli in rock," J. Geophys. Res. **102**, 5281–5293 (1997).

[8] W. M. Visscher, A. Migliori, T. M. Bell, R. A. Reinert, "On the normal modes of free vibration of inhomogeneous and anisotropic elastic objects," J. Acoust. Soc. Am. **90**, 2154–2162 (1991).

[9] K. Lau, and A. K. McCurdy, "Elastic anisotropy factors for orthorhombic, tetragonal, and hexagonal crystals," Phys. Rev. B **58**, 8980–8984 (1998).

[10] N. I. Christensen, "Seismic Velocities," in *Handbook of Physical Properties of Rocks*, edited by R. S. Carmichael (CRC Press, Boca Raton, FL, 1982), Vol. 2, pp. 1–228.

[11] A. L. Fetter and J. D. Walecka, *Theoretical Mechanics of Particles and Continua* (McGraw-Hill, New York, 1980), pp. 226–244.

[12] T. J. Ulrich, and T. W. Darling, "Observation of anomalous elastic behavior in rock at low temperatures," Geophys. Res. Lett. **28**, 2293–2296 (2001).